Pergamon

Int. J. Heat Mass Transfer. Vol. 39, No. 10, pp. 2131–2147, 1996

0017-9310/96 $15.00+0.00

0017-9310(95)00272-3

A thermal model for the rotary kiln including heat transfer within the bed

A. A. BOATENG† and P. V. BARR

Department of Metals and Materials Engineering, The University of British Columbia, Vancouver, B.C., Canada V6T 1Z4

(*Received* 29 *December* 1994 *and in final form* 15 *July* 1995)

Abstract—A mathematical model was developed to predict heat transfer from the freeboard gas to the bed of a rotary kiln. The thermal model incorporates a two-dimensional representation of the bed's transverse plane into a conventional one-dimensional, plug flow model for rotary kilns. The result, a quasi-three-dimensional rotary kiln model, significantly improves the ability to simulate conditions within the bed without the necessity of rigorously accounting for the complex flow and combustion phenomena of the freeboard. The combined model is capable of predicting the temperature distribution within the bed and the refractory wall at any axial position of the kiln. Copyright © 1996 Elsevier Science Ltd.

INTRODUCTION

Rotary kilns are employed by industry to carry out a wide variety of material processing; for example calcining of limestone, reduction of oxide ore, clinkering of cementitious materials, reclamation of hydrated lime, calcining of petroleum coke, etc. This widespread usage can be attributed to factors such as the ability to handle varied feedstock, for example slurries or granular materials having large variations in particle size, or the ability to maintain distinct environments, for example reducing conditions within the bed coexisting with an oxidizing freeboard (Fig. 1). Operators of rotary kilns are not, however, without their problems, for example dust generation, low thermal efficiency and low product quality are some of the typical problems that plague rotary kiln operations. Although the generally long residence time of the material within the kiln, typically one hour or greater, aids in achieving an acceptably uniform product, there is considerable scope for improving this aspect of kiln performance. An initial step toward doing so is to achieve a more quantitative understanding of transport phenomena within the bed material as it passes along the kiln.

In most rotary kiln operations the objective is to drive specific bed reactions which, for either kinetic or thermodynamic reasons, often requires high bed temperatures that, for example in cement kilns, may approach as high as 1200°C. The energy to raise the bed temperature to the required level for reaction and in some instances, for example the endothermic calcination of limestone, to drive the reactions themselves, is extracted from combustion of hydrocarbon fuels in the freeboard. Heat transfer from the freeboard to the bed is rather complex and occurs by all the paths and processes shown in Fig. 1. Perhaps the analytical tools for handling the phenomena occurring within the freeboard space have been readily available, for example the zone method [1] for determining radiative heat transfer or commercial software for calculating fluid flow (and occasionally combustion processes as well), our ability to simulate the freeboard transport phenomena exceeds our ability to accurately determine conditions within the bed. Although numerous rotary kiln models have been proposed [2–6], virtually all of these assume that, at each axial position along the kiln, the bed is well mixed in the transverse plane; i.e. the bed material is isothermal over any transverse section of the kiln. However, many kiln operations experience considerable difficulty in achieving a uniform product, one example being lime kilns which experience chronic problems in preventing dead-burning of larger particles while fully calcining the finer particles. Evidence such as this, as well as operator experience, suggests that a substantial transverse temperature nonuniformity is generated within the bed. Thus the well-mixed assumption, although expedient to the modelling of the rotary kiln, is clearly deficient because it ignores the motion of the bed in the transverse plane or, more precisely, because it ignores the effect of this motion on the redistribution within the bed material of energy absorbed at the bed–freeboard interfacial surfaces.

Heat transfer within the bed material occurs by the same mechanisms as in any packed bed; i.e. particle-to-particle conduction and radiation, as well as interstitial gas-to-particle convection. However, the movement of the granular material superimposes an advective component for energy transport which has the potential to dominate overall heat transfer. The trans-

† Present address: Solite Corporation, P.O. Box 27211, Richmond, VA 23261, U.S.A.

NOMENCLATURE

A	interfacial area [m^2] or effective heat transfer area per unit kiln length [m]
A_o	frequency factor [s^{-1}]
c_p	specific heat capacity at constant pressure [J kg^{-1} K^{-1}]
C_J	jetsam concentration of binary mixture
d_p	particle diameter [m]
D_y	diffusion coefficient [m^2 s^{-1}]
e	emissivity
e_o	void fraction
e_p	coefficient of restitution of particles
g	acceleration due to gravity [m s^{-2}]
g_o	radial distribution function
h	heat transfer coefficient [W m^{-2} K^{-1}]
ΔH_r	enthalpy of reaction [J mol^{-1}]
k	thermal conductivity [W m^{-1} K^{-1}]
k'	enhanced bed thermal conductivity [W m^{-1} K^{-1}]
$\dot{m}$	mass flow rate [kg s^{-1}]
$\dot{m}_{fx}$	max flux [kg m^{-2} s^{-1}]
$\mathbf{P}$	stress tensor
Q	net heat transfer [W m^{-1}]
q_{PT}	flux of pseudo-thermal energy
r	radial distance [m]
R	cylinder radius [m]
T	thermodynamic temperature [K]
$\tilde{T}$	granular temperature [m^2 s^{-2}]
u	velocity parallel to bed surface [m s^{-1}]
z	axial distance [m].

Greek symbols

α	distance from bed's surface to zero velocity line of active layer
β	kiln slope [mm^{-1}]
γ	kinetic energy dissipation due to inelastic collisons
δ	distance from bed's free surface to yield line of active layer
$\dot{\lambda}$	species production rate [mol m^{-3} s^{-1}]
ξ	inclined angle subtended by material (dynamic angle of repose)
ρ	bulk density [kg m^{-3}]
ρ_p	particle density [kg m^{-3}]
σ	Stefan–Boltzmann constant [5.67×10^{-8} W m^{-2} K^{-4}]
ν	solids concentration (solids fraction)
ϕ	static angle of repose of material [rad]
ω	angular velocity [s^{-1}].

Subscripts

ax	axial
AL	active layer
b	bed
cb	covered bed
cw	covered wall
eb	exposed bed
ew	exposed wall
ef	effective
g, fb	freeboard gas
p	particle
pf	plug flow
PT	pseudo-thermal
w	wall
r	radiation
s	surface; solids
shell	outer wall (shell).

verse bed motions in rotary kilns, e.g. cataracting, cascading, rolling, slumping, etc. [7, 8] depend on the rotation rate, degree of fill and rheology of the particles. Although industrial kilns may be operated in the slumping mode, it is usually more desirable to achieve the rolling mode in order to take advantage of improved mixing of particles along with faster surface renewal at the exposed bed surface. For the rolling mode the bed material is characterized by the two distinct regions shown in Fig. 2; the thinner active layer which is formed as the granular material flows down the sloping upper bed surface and the much thicker 'plug flow' region where the material is carried upward by the rotating wall of the kiln. Thus energy imparted by the kiln's rotation is continuously fed into the plug flow region as potential energy which is subsequently released and dissipated in the active layer.

The active layer itself is characterized by vigorous mixing and hence a high rate of surface renewal which promotes heat transfer from the freeboard. The vigorous particle motion may also promote de-mixing, termed segregation, in which smaller particles tend to sieve downward through the matrix of larger particles. During segregation the bed motion tends to concentrate finer material within the core, and material within the core, because it has very little chance to reaching the exposed bed surface for direct heat transfer from the freeboard, tends to a lower temperature than the surrounding material. Thus, segregation tends to counteract advective transport of energy and promotes temperature gradients within the bed. The net effect is not necessarily negative, for example in limestone calcination smaller particles react faster than larger ones (at the same temperature) and therefore the segregation of fines to the cooler core may be essential to obtaining uniform calcination of all particles. This suggests that particle size distribution

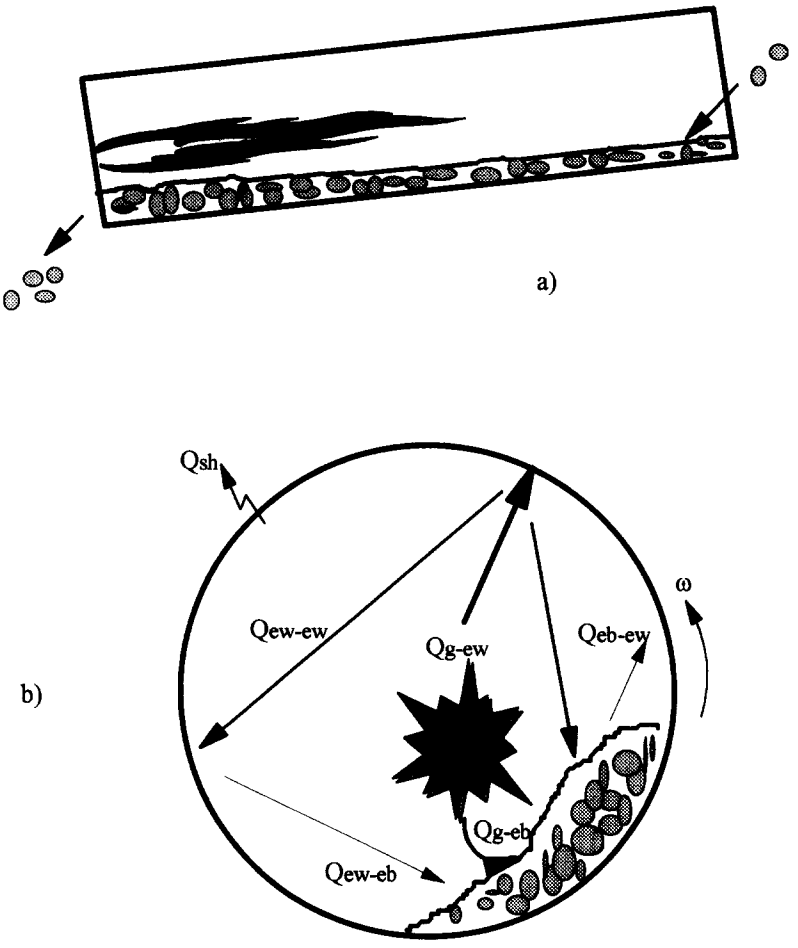

Fig. 1. Schematic of a rotary kiln: (a) axial and (b) cross-section.

in the feed material might be optimized, which again points out the need for developing our predictive capabilities for the bed material.

The objective of the present work was to develop a thermal model for a transverse section of bed material and incorporate this two-dimensional (2D) representation of the bed into a conventional 1D, plug flow type model for rotary kilns. The resultant quasi-3D rotary kiln model would significantly improve our ability to simulate conditions within the bed without the necessity of rigorously accounting for the very complex flow and combustion phenomena of the freeboard. Although the current work focuses on the thermal model for the bed, aspects of the one-dimensional model [6], which is used to generate axial profiles for the mean gas and bed temperatures, and the granular flow model for the bed [9], which is used to determine particle velocity profiles within the bed material, are briefly discussed.

In developing the bed model, the particulate bed material is assumed to behave as a continuum possessing an effective thermal conductivity which is then related to particle size, void fraction and bed temperature using existing particulate bed models. Because particle mixing in the transverse plane of the kiln is at least two orders of magnitude greater than in the axial direction [6], the latter effect is neglected for the bed model. The combined axial and bed model, which is capable of predicting the temperature distribution within the bed and the refractory wall at any axial position of the kiln, is used to examine the role of the various mechanisms for heat transfer over a cross-section of a kiln, for example the regenerative action of the wall and the effect of the active layer (continuously renewing free surface) of bed on redistribution of energy within the bed. The results from the mathematical model are compared with experimental data obtained from a well instrumented 0.41 m i.d. by 5.5 m long pilot kiln.

DESCRIPTION OF THE THERMAL MODEL

The quasi-3D model developed comprises both an axial model (1D) and a cross-sectional model (2D). The former is used to independently determine the 1D axial temperature profiles for the freeboard gas and the bulk bed. Here it is implicitly assumed that the details of the energy redistribution that occurs within the bed do not significantly influence heat transfer between the bed and the freeboard. As part of the

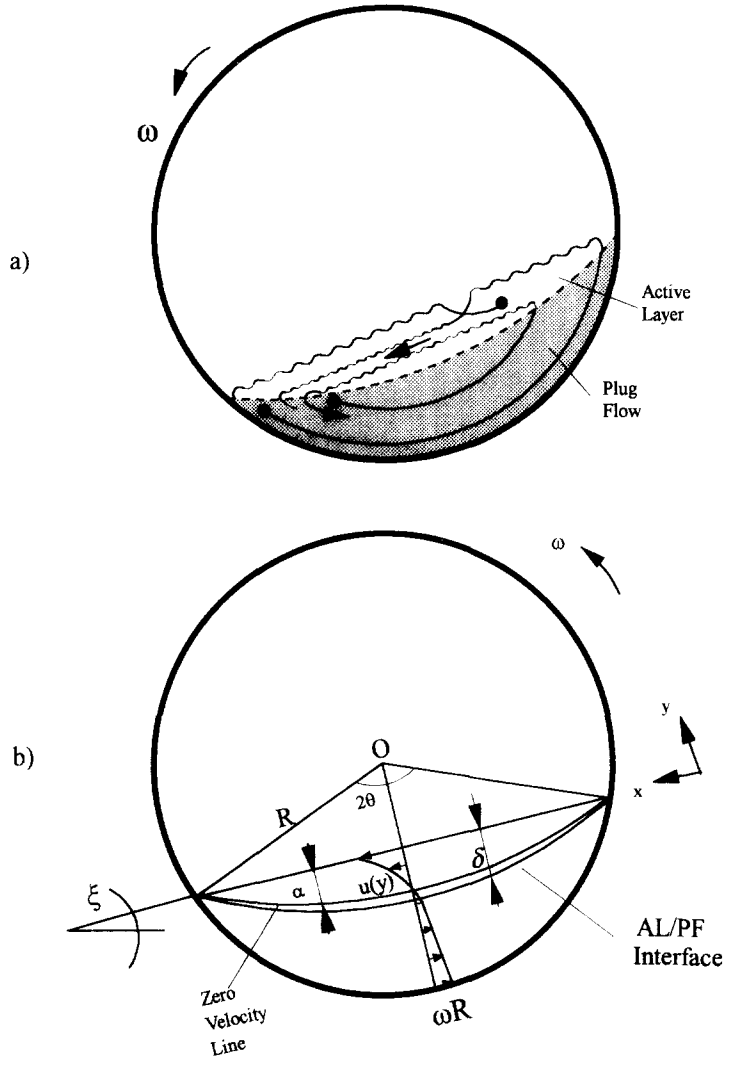

Fig. 2. Granular flow in the transverse plane: (a) a rolling bed motion depicting two distinct regions; (b) calculation domain for a rolling bed.

procedure for calculating these axial temperature profiles, the surface heat flux to the bed is determined and this becomes the thermal boundary condition employed to drive the cross-sectional model. In doing so, the bed temperature gradient computed from the axial model is used as a sink term representing rate of energy removal due to the material flow in the axial direction. This 1D bed temperature is also employed as a check on the mass-averaged temperature which is estimated from the 2D bed model. The 2D model is consequently employed to determine the thermal conditions of the bed material and the refractory wall over successive transverse sections (or slices) of the kiln.

The one-dimensional thermal model applied to the bed and freeboard

Various models for the rotary kiln (see, e.g. [3, 6, 10]) have the capability of predicting 'average' conditions within both the bed and the freeboard as functions of axial position. The thermal component of these 1D models can be derived by considering the transverse slice which divides the section into separate control volumes of freeboard gas and bed material. Under steady-state conditions, and in the absence of any chemical reactions or phase transformations, energy conservation for any control volume requires that

$$\Sigma \dot{m}_g c_{Pg} \frac{dT_g}{dz} = Q_{g \to ew} + Q_{g \to eb} \quad (1)$$

$$\Sigma \dot{m}_b c_{Pb} \frac{dT_b}{dz} = Q_{g \to eb} + Q_{ew \to eb} + Q_{ew \to cb}. \quad (2)$$

One additional condition which must be met is that no net energy accumulation can occur within the wall which yields an auxiliary condition

$$Q_{g\to ew}+Q_{eb\to ew}+Q_{cb\to cw}=Q_{shell}. \quad (3)$$

The system of equations [equations (1)–(3)] can be solved for successive axial positions by any of a variety of techniques (e.g. Runge–Kutta) provided that the various heat transfer terms are characterized in terms of the local gas, bed and wall temperatures. Thus, by starting at either end of the kiln, a complete solution of the thermal problem can be developed. It is chiefly the methodology employed in evaluating the heat transfer terms which distinguishes the various 1D models.

Heat transfer at the interfacial surfaces is complex and involves radiation, convection and, at the covered bed–covered wall interface, conduction as well. Although a heat transfer coefficient can be allocated to each transport path shown in Fig. 1, this should not obscure the difficulty associated with realistic determination of values for these coefficients. As mentioned earlier, in the present work the 1D model is required only to produce a framework from which to operate the 2D thermal model for the bed, and therefore, existing models were used to evaluate heat transfer at the interfaces. In the freeboard, the model developed by Barr *et al.* [6] was utilized to establish coefficients for radiative heat transfer, i.e. $h_{r,g\to ew}$, $h_{r,g\to eb}$, $h_{r,eb\to ew}$, $h_{r,ew\to ew}$. Convection to the exposed wall and exposed bed may be estimated as per Gorog *et al.* [11]. At the covered wall–covered bed interface Schlunder's model [12] was employed which, although perhaps inappropriately complex for the purpose of the present work, takes into account such factors as single particle heat transfer coefficient, wall-to-bed radiation, solid-to-solid heat conduction, and the continuum heat conduction through the gas gap between the bed and the wall surface.

Since there should be no intent to restrict the work to non-reactive conditions in the bed and freeboard, equations (1) and (2) may be expanded to include reactive terms to yield the system;

$$\Sigma \dot{m}_{gi}c_{pgi}\frac{dT_g}{dz}=h_{ew}A_{ew}(T_g-T_w)+h_{eb}A_{eb}(T_g-T_b)+\Sigma\lambda_i A_g\Delta H_{rg} \quad (4)$$

$$\Sigma \dot{m}_{b_j}c_{pb_j}\frac{dT_b}{dz}=h_{eb}A_{eb}(T_b-T_g)+h_{cw}A_{cw}(T_b-T_w)+\Sigma\lambda_j A_b\Delta H_{rb} \quad (5)$$

where λ is the production rate for various species involved in either chemical reactions, for example freeboard combustion, or phase changes each to be determined by the appropriate kinetic expressions.

The two-dimensional thermal model applied to the bed

Although useful results have been obtained from 1D models, the assumption that conditions will be uniform across any transverse section of the bed material will hold only for a well-mixed bed. Since segregation is known to occur within the bed, a 2D model provides an opportunity to examine the effects, on kiln performance, of 'de-mixing' within the bed. Such conditions are driven by the bed motion which is, in turn, established by kiln rotation. However, because no adequate model for this motion has previously appeared, attempts to predict conditions within the bed in 2D or 3D have been rare.

It was mentioned earlier that the rolling bed mode, which is preferred in most kiln operations, comprises two distinct regions (Fig. 2). Because of improved mixing during rolling, it is considered as the mode of operation for the thermal model. In this mode heat transfer within the active layer occurs by conduction (diffusion) and advection (convection). Since flow within the active layer is primarily parallel to the top surface, Cartesian coordinate system was attached to this region for the heat transfer calculations. In order to simplify the analysis, the bed was assumed to consist of a single inert component and to behave as a continuum. Energy conservation for a control volume in the active layer requires that

$$\frac{\partial}{\partial x}\left(k_{ef}\frac{\partial T}{\partial x}\right)-\rho c_p u_x\frac{\partial T}{\partial x}+\frac{\partial}{\partial y}\left(k_{ef}\frac{\partial T}{\partial y}\right)-\rho c_p u_y\frac{\partial T}{\partial y}+\dot{m}_{fx}c_{pb}\frac{dT_{ba}}{dz}=0. \quad (6)$$

It is further assumed that mixing is sufficient to ensure that, within the active layer, the temperature gradient in the axial direction of the kiln (i.e. dT_{ba}/dz in this expression) is uniform. Since, for every kiln rotation the bed material makes three to four excursions in the transverse plane, mixing in this plane is considered far greater than that in the axial direction. Hence the last term in equation (6), which includes the axial gradients of temperature in the active layer, accounts for the removal of energy from the control volume by axial bed flow. It is also assumed that all particles within the active layer advance axially at the same rate and that, because the plug flow region behaves as a rigid body, this axial advance occurs only within the active layer. Thus the mass flux in equation (6) is set by the kiln feed rate and the transverse area of the active layer. In order to solve the equation (6), the convective terms as well as the mixing effects on k_{ef} must be determined by an adequate granular flow model.

In contrast to the active layer, the plug flow region is relatively deep and, since it rotates as a rigid body about the kiln axis, a cylindrical coordinate system was applied to this region as well as the refractory wall itself. Energy conservation for any control volume in the plug flow region and the wall (refractory lining) requires that

$$\frac{\partial}{r\partial r}\left(k_{pf}r\frac{\partial T}{\partial r}\right)+\frac{1}{r^2}\frac{\partial}{\partial\theta}\left(k_{pf}\frac{\partial T}{\partial\theta}\right)-\rho_{pf}c_{p_{pf}}\omega r\frac{\partial T}{r\partial\theta}=0 \quad (7)$$

$$\frac{\partial}{r\partial r}\left(k_w r\frac{\partial T}{\partial r}\right)+\frac{1}{r^2}\frac{\partial}{\partial\theta}\left(k_w\frac{\partial T}{\partial\theta}\right)-\rho_w c_{pw}\omega r\frac{\partial T}{r\partial\theta}=0 \tag{8}$$

where the first two terms constitute the radial and transverse conduction respectively, and the third term represents the movement of energy through the control volume due to the rotation of the kiln. As noted, equation (7) does not include any term for energy transport in the axial direction, it being implicitly assumed that axial conduction in the plug flow region will be negligible and bed particles are assumed to advance axially only in the active layer. The effective thermal conductivity without enhanced mixing was calculated by combining graphical correlations of Diessler and Eian shown in [13] with an inter-particle radiation model by Schotte [14]. The latter is given as

$$k^r=\frac{1-e_0}{\dfrac{1}{k_s}+\dfrac{1}{4\sigma e d_p T^3}}+e_0\sigma e d_p T^3. \tag{9}$$

The flow model applied to the bed

It was mentioned earlier that inadequate granular flow model has been the major setback in expanding 1D models into 2D or 3D. However, the flow behavior in the active (shear) layer of a rotary drum processing granular materials is not significantly different from chute or avalanche flows for which constitutive equations are now available. Experiments conducted in a 1 m rotary drum [9] have shown that at relatively high shear rates constitutive equations of Lun *et al.* [15] combined with that developed by Johnson and Jackson [16] can adequately describe the flow behavior in rotary kilns. In such situations the flow is governed by a field property called granular temperature defined as the kinetic energy per unit mass contained in a random motion of particles [17]. The governing equations for such flows are [15]:

$$\frac{\partial\rho}{\partial t}+\nabla\cdot(\rho u)=0 \tag{10}$$

$$\rho\frac{Du}{Dt}=\rho g-\nabla\cdot\mathbf{P} \tag{11}$$

$$\frac{3}{2}\rho\frac{D\tilde{T}}{Dt}=-\nabla\cdot q_{PT}-\mathbf{P}:\nabla u-\gamma. \tag{12}$$

The stress tensor comprises static and kinetic (streaming plus collisional); the magnitude of each contribution being dependent on rotation rate. Because the flow in the passive (plug flow) region is known ($u=\omega r$), solution to the governing equations is sought only for the active layer. However, the dimensions of this layer are not known *a priori*, so any solution for the particle velocity should include active layer depth. Experiments indicate that the active layer is thin (typically 4% of chord length) therefore a simplified, yet adequate, solution similar to boundary layer flows was sought for the governing equations. This was done by developing integral momentum equations and incorporating into them the stress tensor relations established by [15] and [16]. At high shear rates with sufficient dilation, the momentum equation for bulk solids flow in the active layer may be reduced to [9]

$$\frac{d}{dx}\rho\int_0^\delta(u-u_\delta u)\,dy=\rho g\sin\xi+g_2(v)\rho_p d_p\tilde{T}^{1/2}\frac{du}{dy} \tag{13}$$

where the term $g_2(v)$ relates 'bulk viscosity' to field properties such as the solids fraction (concentration), coefficient of restitution of the particles, particle size, etc. [16]. By applying boundary constraints to the active layer such that $u=0$ @ $y=-\alpha$; u_s @ $y=0$; $u=u_\delta$ @ $y=-\delta$ and relating α/δ to a constant which depends on the material packing, a parabolic profile could be fitted to simultaneously solve for the active layer depth, $\delta(x)$, and $u(y)$. A similar integral equation could not be developed for the granular temperature because of uncertain boundary conditions. However, a representative value for $\tilde{T}$ which is isotropic in y could be found as a function of x by an iteration procedure when solving equation (13). The solution procedure which is detailed elsewhere [9] allows predictions of the velocity distribution in the transverse plane as well as the granular temperature as a function of rotation rate. Having established the granular temperature the self-diffusion coefficient may then be estimated as [18].

$$D_y=\frac{d_p\sqrt{(\pi\tilde{T})}}{8(e_p+1)vg_0(v)}. \tag{14}$$

Figure 3 depicts typical results for the velocity profile at the mid-chord of a 0.41 m i.d drum as function of drum speed (a) and the diffusion coefficient (b). The velocity profiles can be readily used in the convective terms in equation (6). Because of the mixing in the active layer, the effective heat conductance there is greatly enhanced by the granular temperature. The effective thermal conductivity there is therefore modified by a factor relating mass diffusion to heat diffusion, i.e.

$$k'_{ef}=k_{ef}+\rho c_p D_y \tag{15}$$

where D_y is the mass diffusion coefficient computed from equation (14).

The combined axial and cross-sectional model; the quasi-three-dimensional model for the bed

It was mentioned in the opening discussion that the objective of the current work was to examine the role of the bed motion in the transverse plane in determining distribution of energy within the bed. In order to apply this understanding over the entire length of the kiln, the 2D model developed for the bed was combined with the 1D axial model described earlier

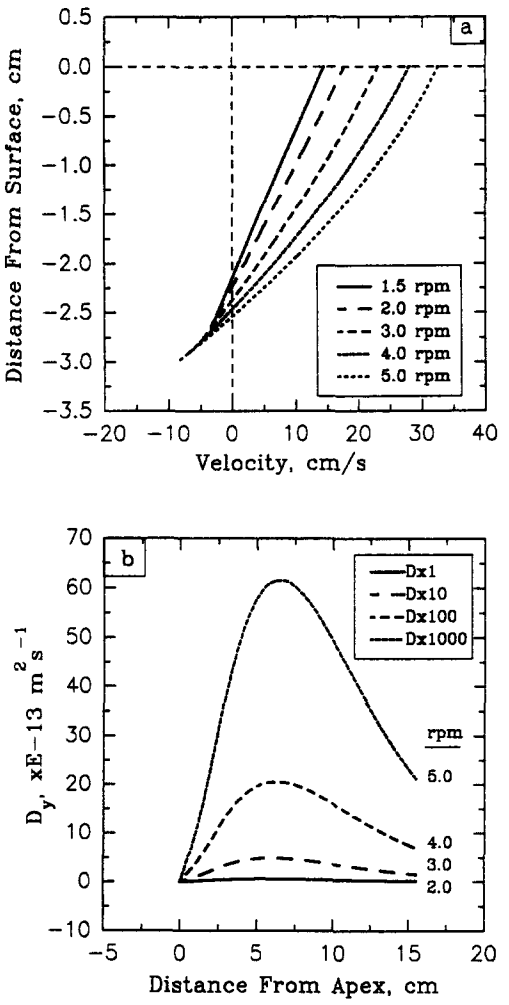

Fig. 3. Typical results for a granular flow model of a pilot (0.41 m diameter) kiln rotating at 2 rpm and 12% fill: (a) velocity profiles at mid-chord; (b) kinetic diffusion in active layer as function of surface position.

to derive a quasi-3D model for the bed material. Although a rigorous 3D formulation of the problem may be accomplished, the extreme aspect ratio of most kilns; i.e. length to diameter ratios, typically 12 : 1 or greater, makes such solution somewhat impractical unless the aspect ratios of the nodal structure are distorted to such an extent that much of the rigor in the axial direction is lost. Therefore the quasi-3D model provides one avenue for predicting conditions within the bed while maintaining relatively modest demands on computing capability.

In the development of the model, asynchronous solution of the 1D and 2D problems was considered. In this approach a 1D solution over the entire kiln length was developed before returning to the charge end to expand the axial bed temperature profile into the transverse plane. Implicit in doing so is the assumption that, at any axial position, heat transfer in the transverse plane (within the bed) will not significantly alter the freeboard, bed and wall. In the case of a 0.41 m i.d. pilot kiln, which will soon be shown, this seems justified.

NUMERICAL SOLUTION

The axial temperature profiles can be developed beginning from either end of the kiln by means of equations (1) and (2) or (4) and (5). However, because most kilns operate as counter-current type heat exchanger, a shooting method [3] must be employed since, when starting at the charge end, the material temperature is known but the gas temperature is unknown. The calculations in the current work were made for an inert bed medium and the freeboard gas was assumed to consist of carbon dioxide and water vapor as the only combustion products. The thermal properties of the gas, as well as the calculation of the gray gas emissivities and absorptivities required for computing the radiative boundary conditions [6] were based on these two gas constituents. As mentioned earlier on, the exit gas temperature and composition are needed to initiate solution (for example, the Runge–Kutta solution procedure) and again, a shooting method may be employed. However, exit gas parameters are easily measurable and input data from experiments help avoid the shooting method (which can destabilize the calculation as a result of the large number of unknown variables involved).

The numerical technique employed to solve the governing bed–wall equations for the cross-section was the control volume-type finite difference described for convective–diffusion equations [19]. The velocity field required for the convective (advective) terms in equation (6) and for the particle size distribution, within a segregated bed, which is required for the evaluation of bed effective thermal conductivity, were provided, respectively, by the granular flow model and an accompanying segregation model [9]. The latter model computes the extent and dimensions of the segregated core development in the cross-section as a result of the flow field and diffusion coefficients such as that shown in Fig. 3.

The grid employed for the 2D calculation domain is shown in Fig. 4. Rectangular grids were used for most of the nodes in the 2D domain except at the interface between the plug flow and the active layer where triangular nodes automatically emerge as a result of the merging of the two coordinate systems. Such nodes were considered as half of the rectangular nodes in the calculation of the nodal areas for heat transfer. The dimension of the active layer shown here is obtained from the flow calculations. Higher density mesh was employed in the active layer of the bed and in the active region of the refractory wall where temperature cycling is expected to occur because of kiln rotation. Although the specific depth of this wall active region is not known *a priori*, temperature measurements by Barr *et al.* [20] suggest that this region does not exceed about 10% of the refractory thickness. Although 10% is used in establishing the

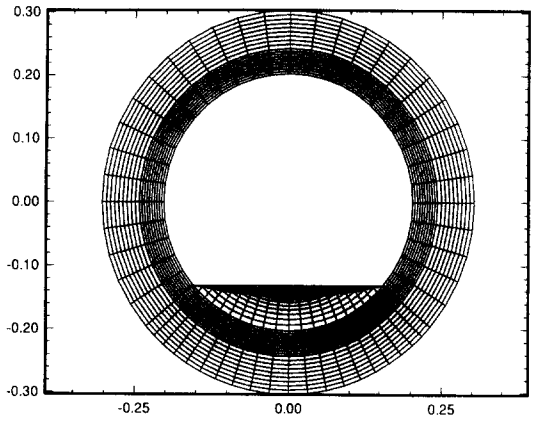

Fig. 4. Grid development for the cross-sectional (2D) thermal model.

mesh, the actual depth automatically results after the numerical calculation is executed. Sensitivity analysis on the mesh for the pilot kiln, 0.41 m i.d., indicated that 15 exposed bed surface nodes were sufficient to produce consistent results. Hence 21 surface nodes were used in all the thermal calculations. Outside the active wall region, the steady-state 1D conduction was applied:

$$Qss = \pi k_w \frac{T_{w_i} - T_{w_i+\Delta r}}{\ln[(r+\Delta r)/r]}. \quad (16)$$

This arrangement of using equation (16) for the remaining 90% of the refractory wall speeds up the numerical calculation which is, otherwise, slow because of the slow thermal response of the refractory lining. The Gauss–Siedal iteration method was employed to solve the system of algebraic equations emerging after discretization with a convergence criterion set as

$$|T_{ij}^n - T_{ij}^{n-1}|_{\max} \leqslant 10^{-5}. \quad (17)$$

The solution requires an under-relaxation technique [19] because of the numerous non-linear temperature dependent terms.

EXPERIMENTAL

Temperature data for model verification were obtained from Barr *et al.* [20] for a 0.41 m i.d. by 5.5 m long pilot rotary kiln located at the University of British Columbia. The facility, which has been described in [20], is instrumented with 66 thermocouples for determining temperatures throughout the freeboard gas, bed material and refractory wall. The experimental program consisted of two parts, the first being a conventional series of trials whereby axial temperature profiles were obtained for the freeboard gas and bed material under prescribed steady-state conditions, as described in [20]. Energy losses through the refractory wall as well as the regenerative action of the inside refractory surface were determined from these trials. In these experiments (trial 1 and trial 2) the bed temperatures were measured with thermocouples that rotate with the kiln wall and so sweep through the bed and the freeboard gas during each kiln revolution. The second set of experiments (trials 3–5) described in [9] employs stationary thermocouples which are imbedded permanently in the bed. The material data and the experimental run conditions used in validating the mathematical models are shown, respectively, in Tables 1 and 2.

VALIDATION OF THE THERMAL MODEL

As mentioned earlier, the current work followed the asynchronous solution of the 1D and 2D problems. Model validation was, therefore, carried out by first comparing the 1D model with axial profiles for the freeboard gas, mean bed temperature and mean wall temperature from the pilot kiln trials. Having validated the 1D model, the heat fluxes determined for the interfaces which will be used in the two-dimensional calculations as boundary conditions, are discussed. In order to check the 2D calculations, 1D profiles were deduced from the cross-sectional temperature distribution for the bed and the wall which were, in turn, compared with either the already validated 1D profiles or the original pilot kiln data. Other validation work includes active wall thermal gradients, steady-state wall temperature gradients, and bed–wall temperature gradients established when the kiln is stopped. This last condition also checks the validity of the continuum assumption for the bed material.

Validation of the one-dimensional model

The 1D model was tested against two inert bed trials (trial 1 and trial 2 of [20]). Input variables for the

Table 1. Relevant physical properties

Property	Sand (fine)	Sand (coarse)	Limestone	Refractory
k[W m^{-1} K^{-1}]	0.268	0.268	0.692	0.400
ρ_{bulk}[kg m^{-3}]	1520	1460	1680	1334
ρ_p[kg m^{-3}]	2627	2627	2483	—
C_p @ 700 K [kJ kg^{-1} K^{-1}]	1.085	1.085	1.137	1.0–1.2
C_p @ 1000 K	1.160	1.160	1.298	1.1–1.3
C_p @ 1300 K	1.195	1.195	1.452	1.2–1.4
Particle size [mm]	0.297–0.841	1.14–3.36	1.0–3.36	N/A

Table 2. Run conditions for pilot kiln trials used in model validation

Trial	Gas flow [kg s^{-1}]	Prim/sec. air [l s^{-1}]	Feed rate [kg s^{-1}]	Fill [%]	Kiln speed [rpm]	Comments
1*	1.97	17.4/43.0	CS/62.0	12	1.5	HT/HF
2*	2.53	18.8/43.0	FS/64.0	12	1.5	HT/HF
3	1.97	17.4/43.0	LS/90.0	27	1.0	LT/LF
4	1.97	17.4/43.0	LS/190.0	27	2.0	LT/LF
5	1.41	—	LS/190.0	27	0	LT/LF

CS = Coarse sand; FS = fine sand; LS = limestone; LT = low temperature; HT = high temperature; LF = low flow; *Barr *et al.* [20].

model were the inlet bed temperature which was set at 50°C and the exit gas temperature (gas temperature at feed end) which was obtained from the experimental data. By using a known exit gas temperature to initiate the computation, the shooting method described earlier for solving the system of equations was avoided. Figures 5(a) and 5(b) provide a comparison of predicted and measured temperature profiles for trial 1 and trial 2, respectively. Agreement between the measured and predicted values was generally good for any gas, bed and wall temperatures. There is expected to be some discrepancy in the bed temperatures near the charge end which may be attributed to uncertain entrance conditions. However, such discrepancies are typical of heat transfer in open tubes where ambient conditions are likely to influence heat exchange at the entrance. Further down the kiln, Ottawa sand undergoes heating during its journey along the kiln as a result of energy exchange with the freeboard gas and the refractory wall. As the material approaches the exit end of the kiln, the temperature difference between the bed and wall dwindles.

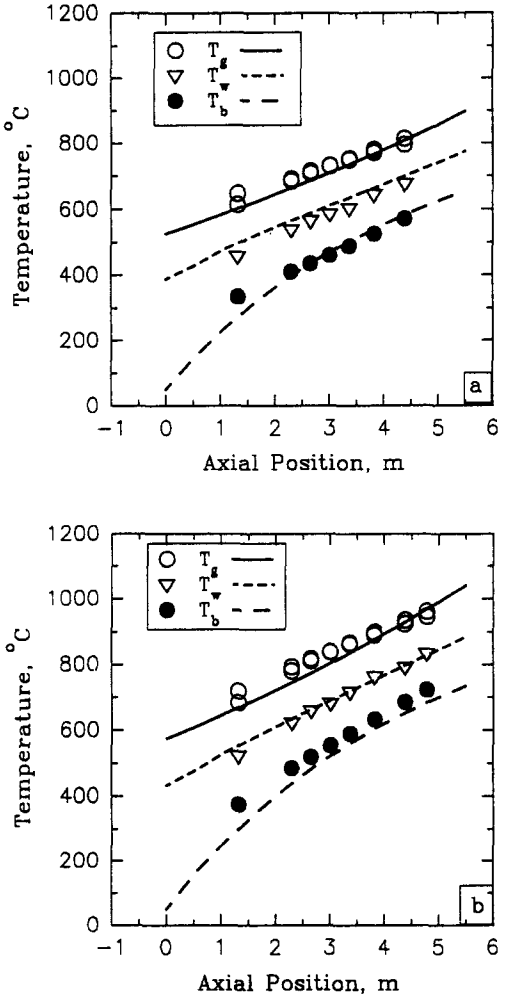

Fig. 5. Predicted and measured mean axial temperature profiles for freeboard gas, refractory wall, and bed burden using 1D model: (a) trial 1, (b) trial 2.

The heat transfer rates at the boundary surfaces for mixed bed are shown in Figs. 6(a) and (b) for trial 1 and trial 2, respectively. Superimposed on the graph is the freeboard gas temperature. These plots indicate that, except at the entrance region, there is a progressive increase in all the interacting heat transfer mechanisms with increased T_g. Although the trends are the same for both trial 1 and trial 2, the magnitudes of the heat transfer rates are slightly higher in trial 2 than in trial 1 as a result of generally higher freeboard gas temperatures. It might be noted that Q_{eb}, the rate of heat transfer to the exposed bed surface, tends to continuously decrease with axial distance from the charge end for trial 2. In addition to Q_{g-eb} the net heat transfer to the exposed bed depends on the radiative exchange between the exposed wall and the freeboard gas, Q_{g-ew}, the exchange between the exposed wall and exposed wall itself, Q_{ew-ew}, and the exchange between the exposed wall and exposed bed, Q_{ew-eb}.

Validation of the cross-sectional model

The initial step in verifying the cross-sectional model was to compare the bed and wall temperatures obtained from this model (using the experimental values of T_g and dT_{ba}/dz as described earlier) against the pilot kiln data. The steady-state 1D profiles shown in Fig. 5 or the measured values may be used to validate the 2D results. However, in order to do so, the mass average bed temperature for each cross-section, along with the arithmetic average surface wall tem-

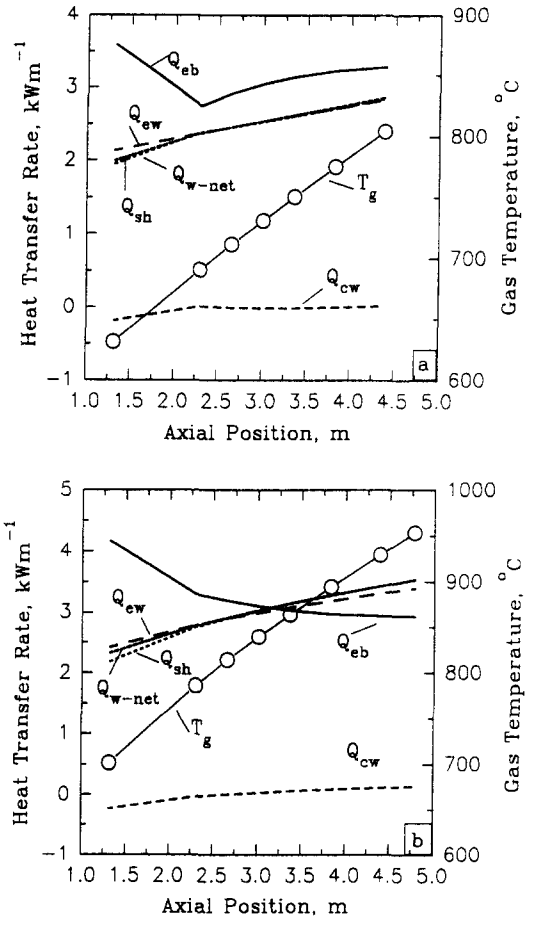

Fig. 6. Predicted heat transfer rates as function of axial position: (a) trial 1, (b) trial 2.

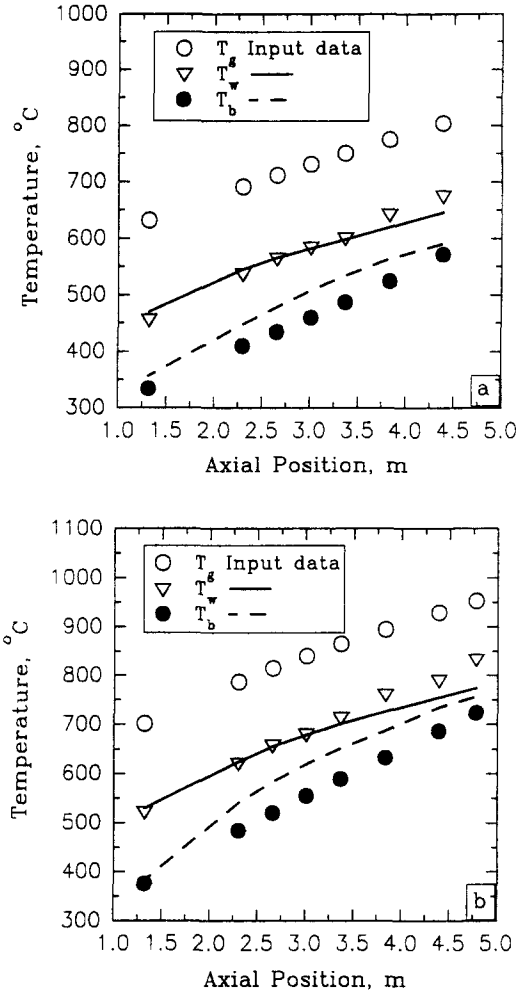

Fig. 7. Predicted and measured average temperatures as function of axial position using 2D model: (a) trial 1, (b) trial 2.

perature, must be calculated from the 2D temperature distribution at each axial position. Figures 7(a) and (b) provide a comparison between the measured bed and wall surface temperature profiles and those predicted by the model (using the measured gas temperatures as input data). Although the predictions are quite satisfactory, it was anticipated that converting 2D results into 1D profiles cannot reproduce the measured temperatures as accurately as the 1D model. Nevertheless, the greatest temperature difference between the model predictions and experiments does not exceed 50°C, which is within limits of experimental error at elevated temperatures. The wall's radial temperature profiles predicted by the 2D model were validated with experimental data in Figs. 8(a) and (b) for trial 1 and trial 2 at three different axial locations (i.e. three freeboard gas temperatures). Also, in Fig. 9(a) the resultant wall steady-state heat losses are presented. As seen from these plots, model predictions are in good agreement with experiment and therefore lend some confidence to the predictions for the temperature distribution in the bed which generated these results and for which data were not available.

In an effort to verify the continuity assumption imposed on the granular bed medium, the two-dimensional model was run for the condition of zero kiln rotation (pilot kiln trial 5) and the results obtained were validated with measured temperature gradients. This is shown in Fig. 9(b). The good agreement between the model predictions and experiment verifies that the model is fundamentally correct prior to rotation and validates the assumption that the bed can be considered as a continuum with effective thermal conductivity. It also provides the opportunity to check how sensitive the convective components would be in distributing energy within the bed.

MODEL APPLICATION

Having established the validity of the 2D model, it was important to describe the effect of the flow of

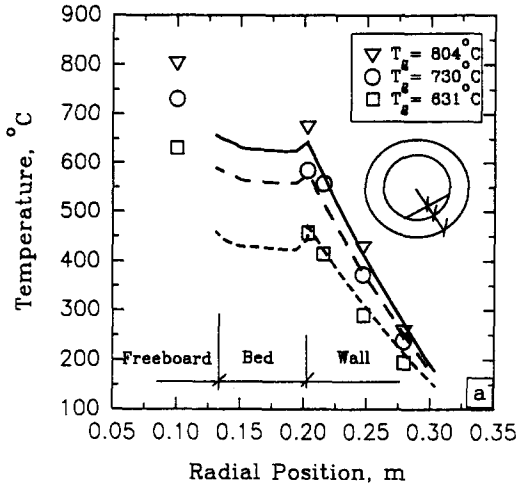

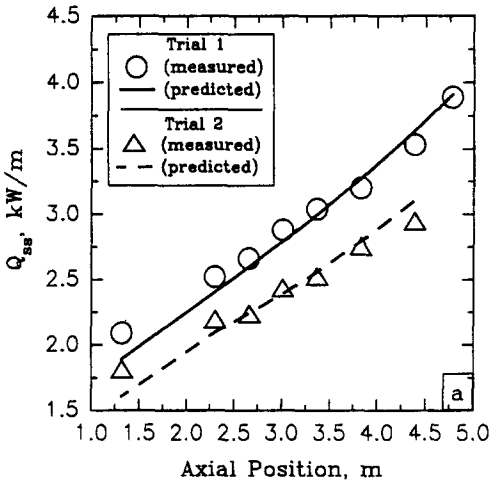

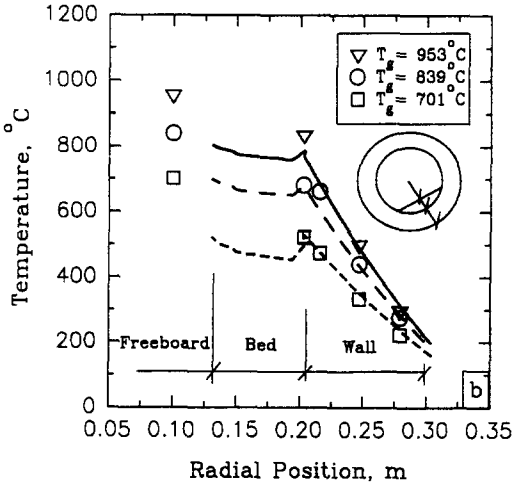

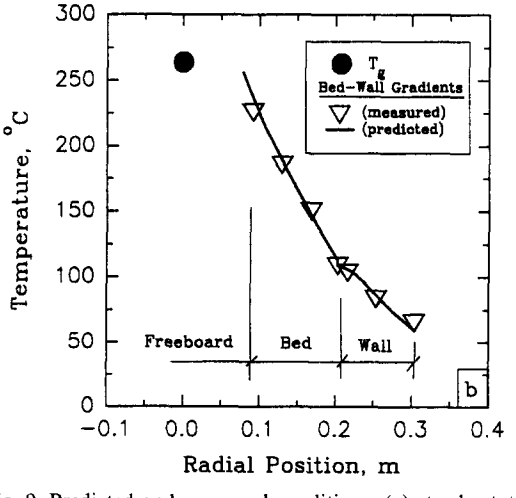

Fig. 8. Predicted and measured temperatures as function of radial position for the refractory wall at several freeboard locations: (a) trial 1, (b) trial 2.

Fig. 9. Predicted and measured conditions: (a) steady-state wall heat loss as function of axial position; (b) temperatures (at mid-chord) for a stationary kiln as function of radial position.

granular material on the temperature distribution. This effect can be established by sensitivity analysis of the various flow factors on the 2D model. These factors include the x-wise and the y-wise velocity components in the active layer, the mass diffusion coefficient resulting from granular temperature calculations, and, in the case of segregating bed, jetsam concentration in the active layer. For purposes of discussion, the flow characteristics may be placed in two categories with respect to what constitutes (i) a 'mixed bed,' and (ii) a 'segregated bed.' The cross-sectional model result depicting temperature distribution within the bed and the refractory lining as a whole is shown in Fig. 10 for a typical well-mixed condition which is sustained at a freeboard gas temperature of 1000°C. Transient response at the lining surface and the periphery of the bed burden due to kiln rotation are evident; the details of which are discussed later.

The well-mixed bed

For this condition the bed motion is assumed to be in the rolling mode and therefore the model implements all the flow results obtained from the granular flow model. The particle size used in the model is assumed uniform and spherical and the diameter is taken as an average of the particle size range used in the experiment which is 0.569 mm for fine Ottawa sand and 2.25 mm for coarse Ottawa sand (Table 1). Figure 11 shows the contour of temperature distribution within the bed cross-section for operational conditions listed under trial 1 with a local freeboard gas temperature of 631°C. Notice from the result of the 1.5 rpm trials that, because of insufficient

mixing (due to slow rotation rate and hence low shear rate), a slight temperature gradient is established between the active layer and the rest of the bed. Also, as a result of the regenerative action of the wall, the bed temperature at the wall is slightly higher than the rest of the bed. However, when the model was run by increasing the rotation rate from 1.5 rpm to 3 rpm, the temperature gradient between the bed surface and the rest of the bed was reduced from 30°C to 12°C and a further increase from 3 rpm to 5 rpm resulted in an isothermal bed. Similar trends were predicted for trial 2 at freeboard gas temperature of 953°C, except that temperature differences between the exposed surface and the rest of the bed were relatively greater than those predicted for trial 1. The increased gradient is attributed to the decrease in particle size as larger sizes tend to enhance inter-particle radiation. In addition, there is a bulk viscosity for granular flow which is directly proportional to solids concentration and shear viscosity. The latter is, in turn, directly proportional to the granular temperature (velocity fluctuations). Therefore, as the shear rate increases with increased kiln speed, granular temperature increases thereby resulting in an increase in the self-diffusion coefficient. The self diffusion coefficient, D_s in the active layer increases by an order of magnitude with an increase in kiln speed and so the effective thermal conductivity increases by the same order of magnitude.

The segregated bed

In order to establish the criteria that result in temperature nonuniformities in a segregated bed, it was assumed that the bed comprises a binary mixture. The effective thermal conductivity is a function of particle size, its magnitude depends upon the concentration gradient for finer particles (jetsam) at each node and is therefore calculated as

$$k_{ef} = C_J(i, j)k_{ef}|_{dp,s} + [1 - C_J(i, j)]k_{ef}|_{dp,l}. \quad (18)$$

Sensitivity analysis shows that when the bed is segregated the y-wise velocity component is virtually negligible and particles travel on an ordered path in the cross section. The flow forms a pattern which is similar to streamlines encountered in laminar flows and diffusional mixing is insignificant due to reduced velocity fluctuations. The thermal results for a segregated bed are shown in Fig. 12. It is evident from this figure that, under these conditions, the region with the lowest temperature (cooler spot) coincides with the segregated core (or kidney) as is anticipated in a strongly segregated rotary kiln bed. Temperature difference between the core and the periphery can be as high as 200°C. Calcination profiles for a strongly segregated limestone bed (A. P. Watkinson, personal communication, 1993) show lower extent of reaction for fine particles at the segregated core than coarse particles at the periphery.

Regenerative heat transfer

The predicted regenerative action of the wall is depicted in Fig. 13. It shows the temperature variation at the covered and exposed wall surfaces [Fig. 13(a)] and the temperature profiles through the lining at the covered wall [Fig. 13(b)]. These predictions show that the wall picks up energy from the freeboard gas and gives it to the bed at the covered wall as the kiln rotates. Therefore, prior to isothermal conditions, the material at the covered wall will always have a higher temperature than the rest of the bed, except perhaps at the exposed bed surface which interacts directly with the freeboard gas. Figure 13(b) indicates that, aside from the regenerative effect, the thickness of the wall active region where temperature cycling occurs and which determines refractory life can be predicted with the model. As seen from the figure, this thickness can be estimated as about 8% of the total wall thickness which agrees with observations made by Barr *et al.* [20].

CONCLUSIONS

The temperature distribution within the bed of a rotary kiln has been investigated by means of a mathematical model which incorporates all the transport phenomena within the bed and the freeboard gas as well.

For mixed bed conditions, typically a rolling bed with uniform particle size, the velocity field that results from kiln rotation, as well as self diffusion, enhances the effective thermal conductivity of the bed and promotes temperature uniformity. The temperature gradients within the bed, for a moderate fill of 12% Ottawa sand in the pilot kiln, at all local freeboard gas temperatures (600–1200°C), do not exceed 30°C for lower rotation rate (typically 1.5 rpm for pilot kilns). Because of strong diffusion effects due to improved granular flow behavior, the bed tends to isothermal conditions at higher kiln rotation rates.

For a segregated bed, which is a condition with marked particle size differences, and also for a condition whereby the flow field suppresses radial diffusion (e.g. slumping bed mode), temperature nonuniformities exist within the bed. Introducing 20% fines into the charge for a pilot kiln at the same operating conditions as a mixed bed, may result in bed surface-to-core temperature difference of over 200°C, with the cooler region coinciding with the segregated core.

Other essential features of the model include the ability to produce accurate temperature distribution of the refractory wall and to provide knowledge on the regenerative action of the wall. The thermal model can be a useful tool in controlling product quality in industrial kilns.

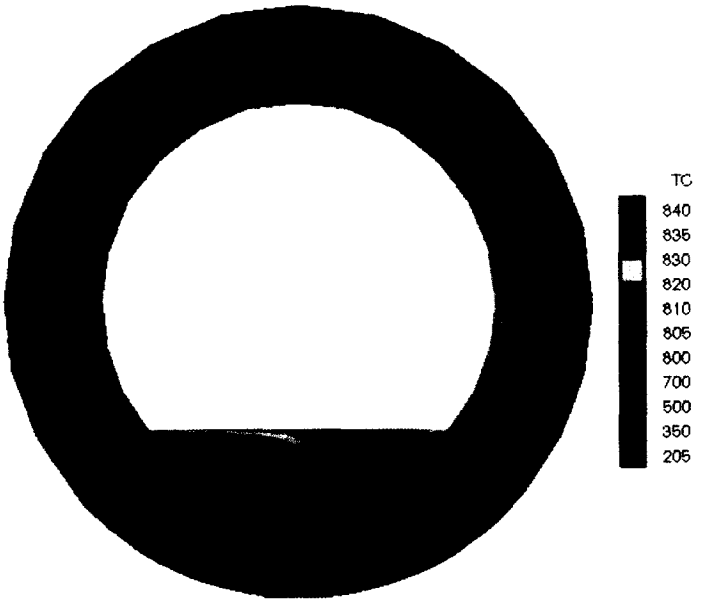

Fig. 10. General result of the 2D model depicting temperature distribution for a well-mixed case at a sustained freeboard gas temperature of 1000°C.

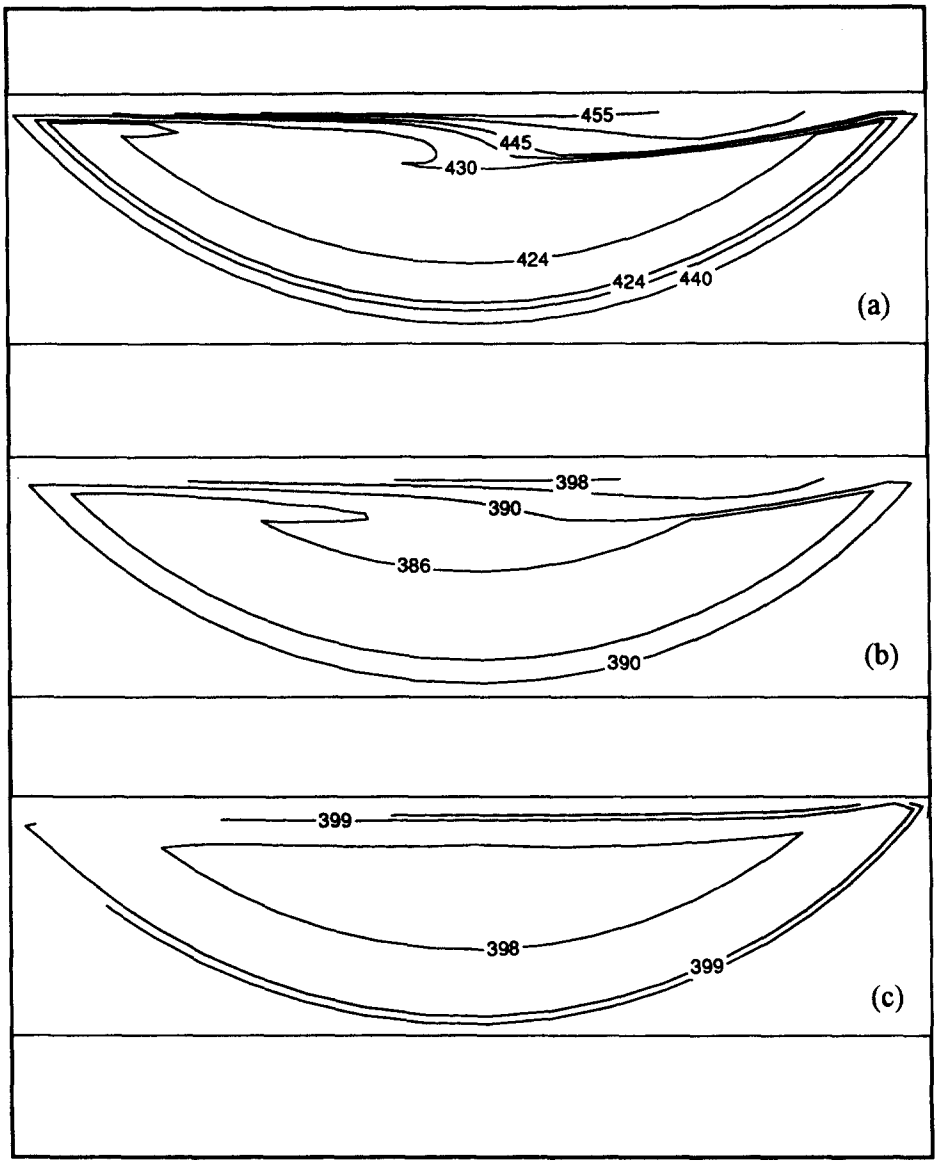

Fig. 11. Detailed plots of bed temperature contours (in °C) predicted for 'mixed bed' with freeboard gas at 631°C: (a) 1.5 rpm, (b) 3 rpm, (c) 5 rpm.

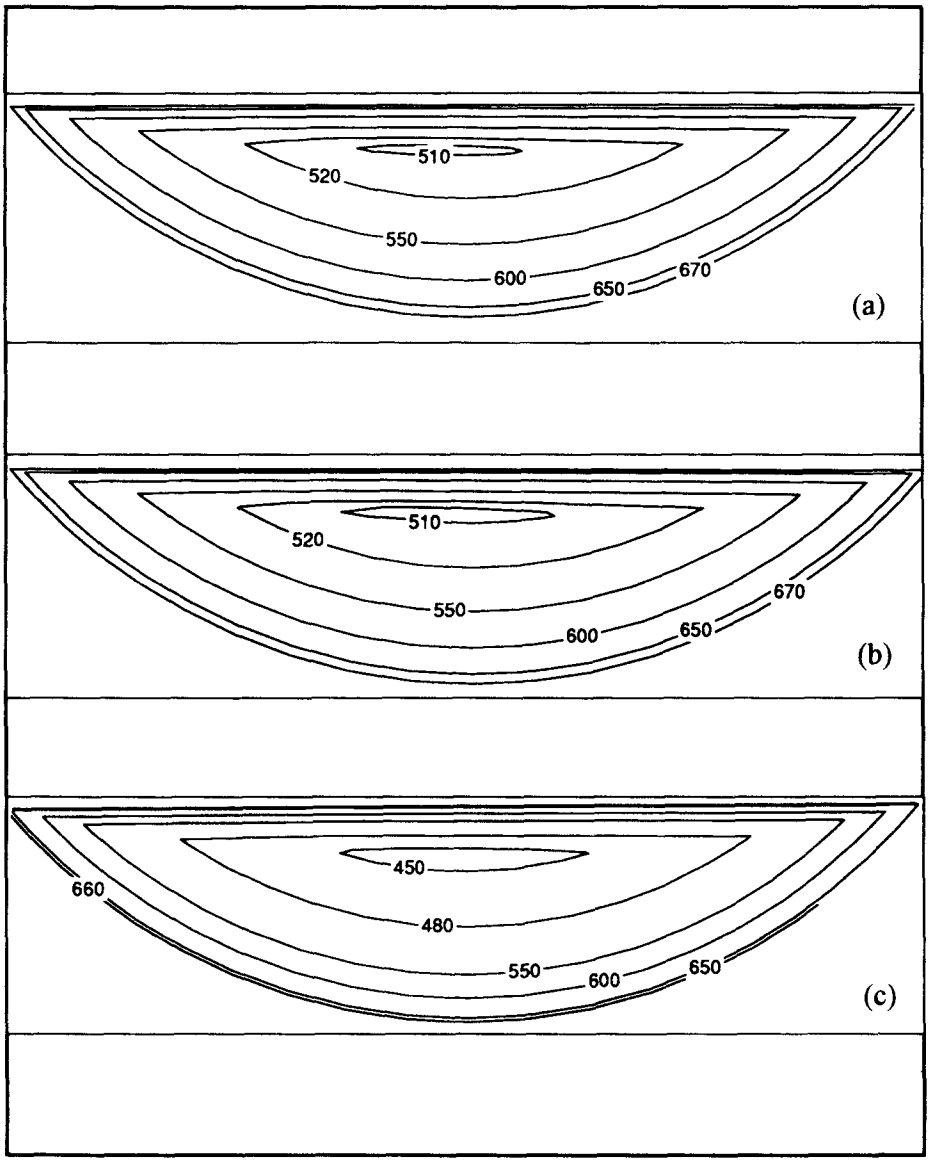

Fig. 12. Detailed plots of bed temperature contours (in °C) predicted for 'segregated bed' with free-board gas at 804 °C: (a) 1.5 rpm, (b) 3 rpm, (c) 5 rpm.

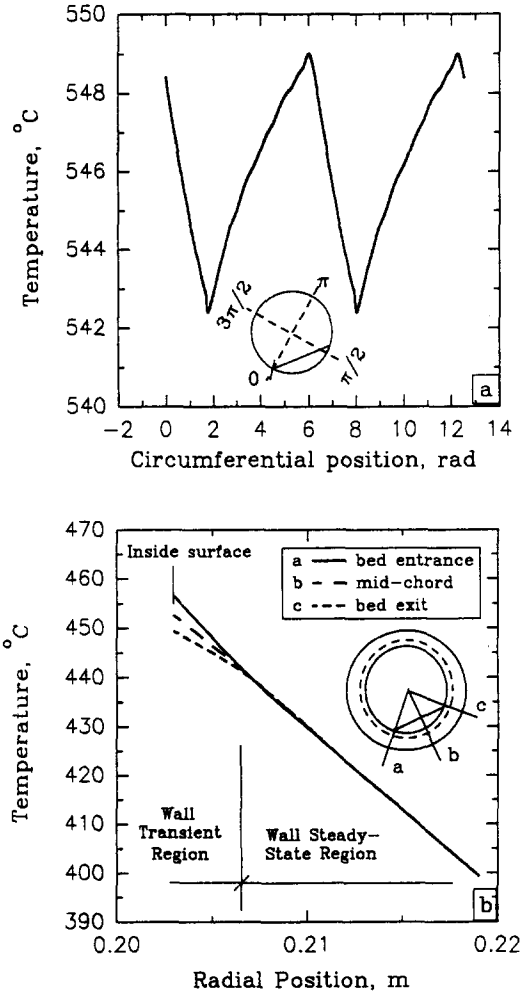

Fig. 13. Regenerative action of refractory wall: (a) cycling wall surface temperatures as function of circumferential position, (b) covered wall temperatures as function of radial position.

Acknowledgements—The authors gratefully acknowledge the cooperation and assistance of Professors J.K. Brimacombe, Director, Centre for Metallurgical Process Engineering, and A.P. Watkinson, Chairman, Department of Chemical Engineering, The University of British Columbia. Financial support for this work was provided, in part, by Alcan and the Natural Science and Engineering Research Council of Canada.

REFERENCES

1. H. K. Guruz and N. Bac, Mathematical modeling of rotary cement kilns by the zone method, *Can. J. Chem. Engng* **59,** 540–548 (1981).
2. G. W. J. Wes, A. A. H. Drinkenburg and S. Stemerding, Heat transfer in a horizontal rotary drum reactor, *Powder Technol.* **13,** 185–192 (1976).
3. S. H. Tscheng and A. P. Watkinson, Convective heat transfer in rotary kilns, *Can. J. Chem. Engng* **57,** 433–443 (1979).
4. J. K. Brimacombe and A. P. Watkinson, Heat transfer in a direct fired rotary kiln—I. Pilot plant and experimentation, *Met. Trans. B,* **9B,** 201–208 (1979).
5. J. P. Gorog, J. K. Brimacombe and T. N. Adams, Radiative heat transfer in rotary kilns, *Met. Trans. B,* **12B,** 55–70 (1981).
6. P. V. Barr, J. K. Brimacombe and A. P. Watkinson, A heat-transfer model for the rotary kiln—II. Development of the cross-section model, *Met. Trans. B,* **20B,** 403–419 (1989).
7. H. Henein, J. K. Brimacombe and A. P. Watkinson, Experimental study of transverse bed motion in rotary kilns, *Met. Trans. B,* **14B,** 191–205 (1983).
8. H. Henein, J. K. Brimacombe and A. P. Watkinson, The modeling of transverse solids motion in rotary kilns, *Met. Trans. B,* **14B** (6), 207–220, (1983).
9. A. A. Boateng, Rotary kiln transport phenomena: study of the bed motion and heat transfer, Ph.D. Dissertation, The University of British Columbia, Vancouver (1993).
10. A. Sass, Simulation of the heat transfer phenomenon in a rotary kiln, *I & EC Process Res. Dev.* **6** (4), 532–535 (1967).
11. J. P. Gorog, T. N. Adams and J. K. Brimacombe, Heat transfer from flames in a rotary kiln, *Met. Trans. B,* **14B,** 411–424 (1983).
12. E. V. Schlunder, Particle heat transfer, *Proceedings of the Seventh International Heat Transfer Conference,* Munchen (1982).
13. P. V. Barr, Heat transfer processes in rotary kilns, Ph.D. Dissertation, The University of British Columbia, Vancouver (1986).
14. W. Schotte, Thermal conductivity of packed beds, *A.I.Ch.E. Jl* **6** (1), 63–67 (1960).
15. C. K. K. Lun, S. B. Savage, D. J. Jeffrey and N. Chepurnity, Kinetic theories for granular flow: inelastic particles in couette flow and slightly inelastic particles in a general flowfield, *J. Fluid Mech.* **140,** 223–256 (1984).
16. P. C. Johnson and R. Jackson, Frictional-collisional constitutive relations for granular materials, with application to plane shearing, *J. Fluid Mech.* **176,** 67–93 (1987).
17. Y. Zhang and C. S. Campbell, The interface between fluid-like and solid-like behaviour in two-dimensional granular flows, *J. Fluid Mech.* **237,** 541–568 (1992).
18. S. S. Hsiau and M. L. Hunt, Kinetic theory analysis of flow-induced particle diffusion and thermal conduction in granular material flows, *J. Heat Transfer* **115,** 541–548 (1993).
19. S. V. Patankar, *Numerical Heat Transfer and Fluid Flow.* Hemisphere, New York (1980).
20. P. V. Barr, J. K. Brimacombe and A. P. Watkinson, A heat-transfer model for the rotary kiln—I. Pilot kiln trials, *Met. Trans. B,* **20B,** 391–402 (1989).